Proceedings Paper:

BENCHMARKING OF CFD MODELLING CLOSURES FOR TWO-PHASE TURBULENT BUBBLY FLOWS

Marco Colombo*[1], Roland Rzehak[2], Michael Fairweather[1], Yixiang Liao[2] and Dirk Lucas[2]

[1]School of Chemical and Process Engineering, University of Leeds,
Leeds LS2 9JT, United Kingdom
[2]Helmholtz-Zentrum Dresden - Rossendorf, Institute of Fluid Dynamics,
Bautzner Landstrasse 400, D-01328 Dresden, Germany
*M.Colombo@leeds.ac.uk

ABSTRACT

Eulerian-Eulerian computational fluid dynamic models are used in the prediction of multiphase gas-liquid flows in nuclear reactor thermal hydraulics and in many other chemical and process engineering applications. The modelling approach, based on the concept of interpenetrating continua, allows the calculation of complex and large-scale industrial flows with a relatively limited computational load. However, interfacial transfer processes need to be entirely modelled through numerous closure relations. A large number of different optimized closure sets are available, each often showing remarkable accuracy, but generally only over a few experimental data sets. This specificity makes it difficult to compare the overall accuracy of the models and obstructs the development of more general and robust approaches. In this paper, the bubbly flow models developed at the University of Leeds and the Helmholtz-Zentrum Dresden - Rossendorf are benchmarked against relevant experiments. These two research groups follow a similar modelling approach, aimed at identifying a single universal set of widely applicable closures. The models, implemented respectively in Star-CCM+ and CFX, are applied to a large selection of bubbly flows in different geometries. The main focus is on the momentum transfer, mainly responsible for the lateral bubble distribution in any flow, and on turbulence closures. Therefore, monodispersed bubbly flows that can be effectively characterized with a single average bubble diameter are selected. Overall, the models are found to be generally reliable and robust, and additional developments towards further improved accuracy, increased generality and the definition of a common unified set of model closures are identified. In future, additional benchmark exercises of this kind will be performed, and potentially the definition of proven sets of reference experiments will be recommended.

KEYWORDS
CFD, bubbly flows, two-fluid model, baseline closure, void distribution, two-phase turbulence

1. INTRODUCTION

Bubbly flows are frequently encountered in industrial equipment and processes in many engineering fields, such as nuclear reactor thermal hydraulics, chemical and process engineering applications, oil and gas, biotechnology and pharmaceutical processes, to name a few. The hydrodynamics of bubbly flows is challenging due to the complex interactions between the continuous liquid and the dispersed gas phase. When the bubble volume fraction becomes significant, bubble collision and coalescence are also no longer negligible, and add further complexity by continuously altering the bubble diameter distribution in the flow. In view of the difficulties encountered in the modelling of bubbly flows with empirical or semi-empirical treatments, computational fluid dynamics (CFD) has been the subject of extensive research

in recent years [1-7]. CFD offers the potential to handle the multiscale nature of bubbly flows by accounting for the local small scale physical effects that drive the macroscopic behaviour of the flow.

Generally, the prediction of bubbly flows of industrial relevance relies on two-fluid Eulerian-Eulerian models [2, 4-6, 8, 9]. The two-fluid modelling approach is based on the concept of interpenetrating continua. The local instantaneous field is averaged and the model solves the temporal and spatial distribution of the volume concentration of the different phases. Therefore, individual bubbles and their interfacial details are not resolved, and all the interfacial interactions require additional modelling through a number of closure relations. Amongst these, a notable amount of work has been focussed on closures for the forces acting between the fluid and the bubbles that impact bubble motion and the spatial void fraction distribution [6, 9].

A very well-known and not entirely resolved challenge concerns the lateral distribution of bubbles that flow in closed ducts such as pipes or channels. If the bubbles are sufficiently small, their shape remains close to spherical and, in upflow, the shear lift force acting perpendicularly to the bubbles' main direction of motion pushes the bubbles towards the duct wall. With increases in size, the bubbles acquire an ellipsoidal shape as a consequence of the increased deformation induced by the surrounding fluid. The shear lift acting on these bubbles reverses its direction and pushes them towards the centre of the channel. Research on the subject, for air-water flows under normal conditions, suggests that this change in sign of the lift force occurs for bubbles with diameters between 5 and 6 mm [10]. In bubbly flows of mainly spherical bubbles, the lateral void fraction distribution shows a distinctive peak near the wall. This has been generally considered to be a consequence of an additional lift force, simply referred to as the wall force, which pushes bubbles away from a wall and thus prevents them moving closer to it [11-13]. In two-fluid CFD models, the wall-peak in the void fraction is obtained from the combined action of the shear lift force and the wall force. Over the years, although different models have demonstrated a good accuracy, numerous lift and wall force formulations have been developed, often optimized over a limited amount of data [14] or, more correctly, numerous optimized coupled lift-wall force models exist. Clearly, this significantly affects the robustness and general applicability of two-fluid models and makes comparisons of the overall accuracy of different models difficult.

In recent years, a different approach is emerging, driven by the necessity to develop models that are robust and generally applicable, even if at the expense of a slight decrease in accuracy over single experiments. Researchers at the Helmholtz-Zentrum Dresden - Rossendorf (HZDR) have introduced their baseline closure strategy [5, 9, 15], in which a default set of closure relations has been selected to cover all the most important physical processes impacting on bubbly flows. These were systematically validated over a continuously increasing experimental database, demonstrating the overall accuracy and the applicability of the models. Each single closure would be modified only after proving that any change benefitted the prediction of the entire database and not only a small sample of data [16]. A similar strategy has been adopted in recent developments at the University of Leeds (UoL), where the developed two-fluid CFD model has been validated over a large set of bubbly flow measurements [8].

This paper is the first from an ongoing benchmarking activity of the CFD models developed at UoL and HZDR against a wide range of experimental data, starting with adiabatic bubbly pipe flows. Through these comparisons, the authors aim to identify the strengths and weaknesses of each model, and areas where joint developments can be more beneficial to the future development of an accurate and generally applicable unified model. The models are implemented in two different codes, STAR-CCM+ and CFX. The benchmark was blind and we did not make any changes to the models before application to predicting an experimental dataset which was built from three available literature databases. For UoL, in addition to the

original version of their overall model, a more recent model based on an elliptic blending Reynolds stress turbulence model (EB-RSM) is evaluated. The model resolves the near-wall region and follows from recent findings suggesting a significant impact of turbulence in the liquid phase on the void fraction distribution [17]. In addition to interfacial closures, and in view of the different turbulence closures adopted, the other main subject of the paper is turbulence modelling. This is also a very active and progressing area of research, with numerous two-equation [5, 6] and Reynolds stress [8, 17] turbulence models being proposed, with an increasing focus on the modelling of the bubble-induced turbulence contribution [8, 18]. To focus on these aspects, experiments with monodispersed bubble distributions, which can be effectively characterized with a single fixed value of the average bubble diameter, were selected. The paper starts from the experiments selected. Subsequently, the CFD models employed are illustrated and the results discussed.

2. EXPERIMENTS

A number of experimental bubbly flows databases have been made available. In this paper, we have built a dataset of six experiments selected from the studies of Hosokawa and Tomiyama [4], Liu [19] and the MTLoop facility [20], the latter built and operated at HZDR over the last couple of decades. All the experiments have an essentially monodispersed bubble distribution. Therefore, the use of a population balance model to account for bubble breakup and coalescence can be avoided and the work described can be entirely focused on interfacial forces and turbulence closures. More specifically, almost every experiment shows a marked void fraction peak near the wall.

Hosokawa and Tomiyama [4] studied a vertical upward flow of water with air bubbles at atmospheric pressure and temperature in a vertical pipe of inside diameter 25 mm. Laser Doppler velocimetry and shadowgraphy were used to measure radial profiles of the liquid and gas velocities, the gas volume fraction and the liquid turbulence kinetic energy at an axial location L/D = 68. From stereoscopic images of the bubbles obtained with two high-speed cameras, the authors reconstructed the bubble number, size and shape. Measurements were obtained in the ranges 0.5-1.0 m s^{-1} for the liquid superficial velocity, 0.018-0.036 m s^{-1} for the air superficial velocity, 0.0146-0.0399 for the void fraction and 3.21-4.25 mm for the bubble diameter. Superficial velocities and measured average values of the void fraction and the bubble diameter were used to setup the CFD simulations.

Liu [19] studied vertical upward air-water bubbly flows at atmospheric pressure and a temperature of 26˚C in a pipe of 57.2 mm inside diameter. Axial profiles of liquid velocity, turbulence intensity, gas fraction and the average bubble diameter were measured at an axial position L/D = 60 with a dual resistivity probe and a single hot film anemometry probe. In the simulations, void fraction was imposed from the averaged values obtained by integration of the radial profiles. These same average values were used to adjust the value of the air superficial velocity to achieve the correct flux of air through the pipe cross-section at the measurement position.

The MTLoop facility [20] was built to study the development of upward vertical flows of air and water in a pipe of inside diameter 51.2 mm. Experiments were performed at atmospheric pressure and 30˚C. Radial profiles of the gas volume fraction and average velocity, and the bubble size distribution, were measured at different heights from the inlet to L/D = 60, using a wire-mesh sensor. Two cases showing a clear wall-peaked void fraction distribution were selected. Average bubble diameter and void fraction from the last measuring station were used in the CFD simulations. As before, average void fraction was also used to adjust the nominal value of the gas superficial velocity. A summary of the experimental conditions and the averaged values is provided in Table I.

Table I. Experimental cases selected for the CFD simulations.

Experiment	j_w [m s^{-1}]	j_a [m s^{-1}]	$<\alpha_g>$ [-]	$<d_B>$ [mm]	D [m]
H12 [4]	0.5	0.025	0.0399	4.25	0.025
H21 [4]	1.0	0.2	0.0146	3.52	0.025
L11A [19]	0.5	0.12	0.152	2.94	0.0572
L21C [19]	1.0	0.13	0.096	4.22	0.0572
MT041 [20]	1.017	0.012	0.01	4.9	0.0512
MT061 [20]	0.405	0.031	0.0503	5.2	0.0512

3. CFD MODELS

The CFD models are based on the two-fluid Eulerian-Eulerian approach. The flow is adiabatic, and averaged continuity and momentum equations are solved for each phase [21, 22]. Interfacial momentum transfer between the phases is modelled by a set of closure relations that account for the different forces that act on the bubbles.

3.1 Interfacial forces

In the HZDR model the drag force, lift force, wall force, turbulent dispersion force and virtual mass are all considered. The same forces are modelled in the UoL code, except for virtual mass that is neglected. In the context of the present work, focused on steady parallel flows, no differences are expected by including or neglecting the virtual mass.

The drag force quantifies the resistance that the surrounding liquid imposes on bubble motion. In the HZDR model, the drag coefficient C_D is obtained from the model of Ishii and Zuber [23] as a function of the bubble Reynolds number Re (calculated from the relative velocity between the fluid and the bubble U_r, the fluid kinematic viscosity v and the pipe diameter D, as Re = U_r D / v) and the Eötvös number Eo (Eo = $\Delta \rho g D^2 / \sigma$, where $\Delta \rho$ is the density difference, g the gravitational acceleration and σ the surface tension):

$$C_D = max\left(C_{D,sphere}, min\left(C_{D,ellipse}, C_{D,cap}\right)\right) \quad (1)$$

$$\begin{cases} C_{D,sphere} = \dfrac{24}{Re}(1 + 0.1Re^{0.75}) \\ C_{D,ellipse} = \dfrac{2}{3}\sqrt{Eo} \\ C_{D,cap} = \dfrac{8}{3} \end{cases} \quad (2)$$

In UoL model, the drag coefficient is instead calculated from the theoretical formulation of Hosokawa et al. [24] that accounts for the effect of the bubble aspect ratio E:

$$C_D = \frac{8}{3}\frac{Eo}{E^{2/3}(1-E^2)^{-1}Eo + 16E^{4/3}}F^{-2} \quad (3)$$

In Eq. (3), F is also a function of the bubble aspect ratio [4]. Following experimental evidence of an aspect ratio close to 1 near a solid wall, E is determined from the following expression [4]:

$$E = max\left[1.0 - 0.35\frac{y_w}{d_B}, E_0\right] \quad (4)$$

Here, y_w is the distance from the wall and the reference aspect ratio E_0 is obtained from Welleck et al. [25]. An additional correction factor is included to account for the effect that neighbouring bubbles have in altering the velocity field:

$$C_D = C_{D,0}\alpha^{-0.5} \tag{5}$$

The lift force expresses the force perpendicular to its direction of motion that a bubble experiences when travelling in a shear flow. For a spherical bubble, the lift coefficient is positive and the bubble travels in the direction of decreasing liquid velocity. In the HZDR model, this coefficient is obtained from the correlation of Tomiyama et al. [10], obtained from the trajectories of single air bubbles rising in a shear flow of a glycerol water solution:

$$\begin{cases} C_L = min[0.288tanh(0.121Re), f(Eo_\perp)] & Eo_\perp < 4 \\ C_L = f(Eo_\perp) & 4 < Eo_\perp < 10 \\ C_L = -0.27 & Eo_\perp > 10 \end{cases} \tag{6}$$

In the previous equation, $Eo_\perp$ is the Eötvös number calculated from the maximum horizontal dimension of the bubble, which is determined using the same aspect ratio correlation from Welleck et al. [25] as used for E_0 in Eq. (4). The Tomiyama et al. [12] model predicts the change of sign in the lift coefficient for cap bubbles at $d_B \sim 6$ mm. In the UoL model, the lift coefficient is assumed constant and equal to 0.10, which was found to be reasonably accurate over a significant range of experiments [8]. However, when the EB-RSM is employed, and as a consequence of the much more refined numerical solution mesh near the wall, very high lift values would be predicted in the small cells adjacent to the wall and at a distance much smaller than the bubble diameter. Therefore, and in the absence of a physically based approach, the lift force is decreased near the wall, to approach zero at the wall, using the correlation from Shaver and Podowski [26]:

$$C_L = \begin{cases} 0 & y_w/d_B < 0.5 \\ C_{L0}\left[3\left(2\dfrac{y_w}{d_B}-1\right)^2 - 2\left(2\dfrac{y_w}{d_B}-1\right)^3\right] & 0.5 \leq y_w/d_B \leq 1 \\ C_{L0} & y_w/d_B > 1 \end{cases} \tag{7}$$

When a bubble moves near a wall in a quiescent liquid, it experiences an additional wall lift force, often referred to as the wall force, which drives the bubble away from the wall. In the HZDR model, the wall coefficient is calculated from Hosokawa et al. [12], who derived a model based on the trajectories of single bubbles in the range $2.2 \leq Eo \leq 22$:

$$C_W = f(Eo)\left(\frac{d_B}{y_w}\right)^2 \tag{8}$$

where

$$f(Eo) = 0.0217Eo \tag{9}$$

In the model of UoL, the wall force coefficient is instead evaluated from the model of Antal et al. [11]:

$$C_W = \max\left(0, C_{W,1} + C_{W,2}\frac{d_B}{y_w}\right) \tag{10}$$

The coefficients were taken as $C_{W,1}$ = -0.65 and $C_{W,2}$ = 0.45 [8]. The physical basis of this model, based on wall lubrication theory, has been recently questioned [27], as has its accuracy

[13]. In the more recent version of the UoL model, based on the EB-RSM, no wall force is included.

The turbulent dispersion force accounts for the effect of velocity fluctuations in the continuous phase on the bubbles. In both models, this is modelled using the approach of Burns et al. [28] who derived an expression based on Favre averaging of the drag force. In the HZDR model, virtual mass is also accounted for and the virtual mass coefficient is fixed at C_{VM} = 0.5 [6].

3.2 Turbulence modelling

In view of the low density of the dispersed phase, turbulence is modelled in the continuous phase only and the value in the dispersed phase is then derived from the continuous phase turbulence field using:

$$\mu_{t,a} = \frac{\rho_a}{\rho_w} C_t^2 \mu_{t,w}$$ (11)

Here above, μ_t is the turbulent dynamic viscosity and C_t is assumed equal to 1 in the UoL models. In the HZDR model, the turbulent viscosity is taken equal to zero with negligible effects expected on the results. The HZDR model adopts the two-equation k-ω SST model, which couples the advantages of the k-ω model near the wall and the k-ε formulation away from it [29]. The model includes specific source terms in the equations for turbulence kinetic energy, k, and the specific rate of dissipation, ω, to model the bubble-induced contribution to turbulence. The bubble-induced turbulence kinetic energy production is derived from the approximation that the energy lost by the bubbles due to drag (**F$_D$**) is converted into turbulence kinetic energy in the wake of the bubble [18]:

$$S_k^{BI} = \boldsymbol{F_D U_r}$$ (12)(1)

The corresponding source of the turbulence energy dissipation rate, ε, is obtained by dividing Eq. (12) with an appropriate timescale τ:

$$S_\varepsilon^{BI} = \frac{C_{\varepsilon,BI}}{\tau_{BI}} S_k^{BI}$$ (13)

This timescale, following Rzehak and Krepper [18], is obtained from the length scale of the bubble and the velocity scale of the turbulence in the continuous phase, τ = d$_B$ / k$^{0.5}$. This source term is then transformed into an equivalent ω-source. The $C_{\varepsilon,BI}$ coefficient is taken equal to 1. Since bubble-induced turbulence is modelled through the source terms, the turbulent viscosity is still obtained from the single-phase definition:

$$\mu_t = C_\mu \rho \frac{k^2}{\varepsilon}$$ (14)

with C_μ = 0.09. The original UoL model uses a multiphase version of the SSG RSM model of Speziale et al. [30], where the pressure strain relation Φ is quadratically non-linear in the anisotropy tensor. The model from now on will be referred to as UoL SSG. In the more recent version, the model employs the elliptic blending Reynolds stress formulation [31] and hence is referred to as UoL EB. In this model, the near-wall region is resolved by imposing the correct asymptotic behaviour of the pressure strain relation:

$$\Phi_{ij}^w = -5\frac{\varepsilon}{k}\left[\overline{u_i u_k} n_j n_k + \overline{u_j u_k} n_i n_k - \frac{1}{2}\overline{u_k u_l} n_k n_l (n_i n_j + \delta_{ij})\right]$$ (15)

In the previous equation, $u_i u_j$ are the components of the Reynolds stress tensor and n_i the components of the unit vector directed towards the wall. Transition from near-wall behaviour to the SSG model away from the wall is obtained by means of an elliptic relaxation function α_{EB}:

$$\Phi_{ij} = (1 - \alpha_{EB}^3)\Phi_{ij}^w + \alpha_{EB}^3 \Phi_{ij}^h \qquad (15)$$

A similar blending is also performed for the turbulence energy dissipation rate and the relaxation function is obtained by solving an elliptic relaxation equation [31]. Both the UoL SSG and the UoL EB models adopt the bubble-induced turbulence model given by Eqs. (12) and (13), with the only difference being that the k source is multiplied by a constant factor equal to 0.25. After being calculated, this is subdivided between the three normal stresses, with a larger portion assigned to the axial stress following the solution for a potential flow around a sphere [32]. Following [8], in this work the relative contribution assigned to the axial component is slightly increased with respect to the potential flow solution and reaches 50% of the total bubble induced source. A summary of the various models is provided in Table II.
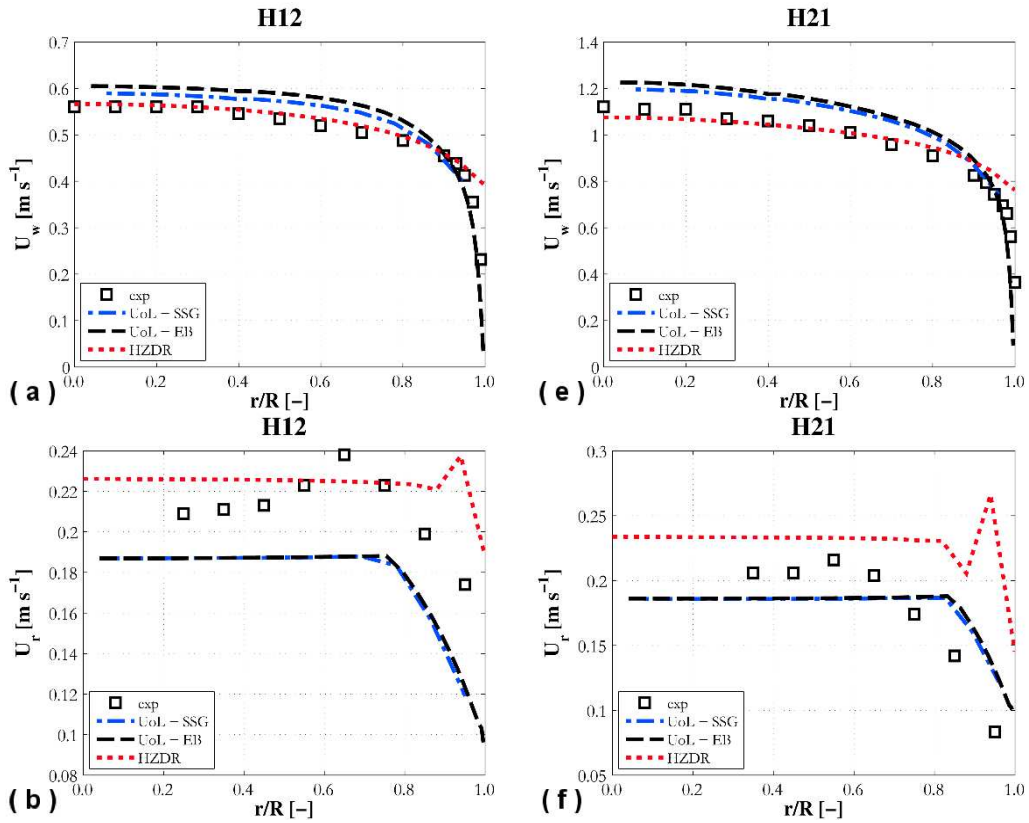
3.3 Numerical solutions method

The HZDR model was solved using a customized version of ANSYS CFX [33]. A high resolution scheme was used to discretize the advection terms. Simulations were run in time until steady-state conditions were reached and a second-order backwards Euler scheme was used for the temporal discretization. The gas fraction coupling was resolved using the coupled solver option, and further details can be found in the ANSYS CFX documentation [33]. At the wall, the no-slip boundary condition was imposed for the liquid phase and the free-slip boundary condition for the gas phase. The velocity in the first near-wall cell was imposed using the single-phase wall law for a smooth wall. At the inlet, the velocity of the phases and void fraction were imposed based on the experimental measurements (adjusted if required, as discussed in Section 2). The average bubble diameter is kept fixed and also taken from the experimental measurements. A fixed pressure boundary condition was used at the outlet. A narrow axisymmetric section of each pipe was simulated and a mesh independence study ensured that grid independent solutions were achieved, while the distance from the wall of the first grid point was sufficient to ensure the validity of the law of the wall.

The UoL models were solved using the STAR-CCM+ code [34]. A second-order upwind scheme was used for the convective terms and a second-order implicit scheme was employed to advance the simulation in time. The pressure velocity coupling was solved with a multiphase extension of the SIMPLE algorithm. The same boundary conditions enforced in the HZDR model were used, except for the gas velocity at the wall, for which a no-slip boundary condition was imposed. The velocity in the first near-wall cell is obtained from the single-phase law of the wall for the UoL SSG model. In the UoL EB model, the wall region is resolved and, at the wall, the turbulent stresses are set to zero while, for the turbulence dissipation rate, the asymptotic limit $\varepsilon = 2v(k / y_w)_{yw \to 0}$ was imposed [31]. Values of inlet velocities, void fraction and average bubble diameter were equal to those used in the HZDR model. A 1/4 section of each pipe was simulated and mesh independence studies ensured that grid independent solutions were obtained for both models. The UoL EB model, because of the grid refinement required at the wall, employed meshes with a significantly greater number of elements. For example, while a 12,600 element mesh was sufficient for the Hosokawa and Tomiyama [4] pipe with the UoL SSG model, the UoL EB model required 220,800 elements for the same geometry, resulting in a significant increase in the required computational time.

Table II. Summary of sub-model closures.

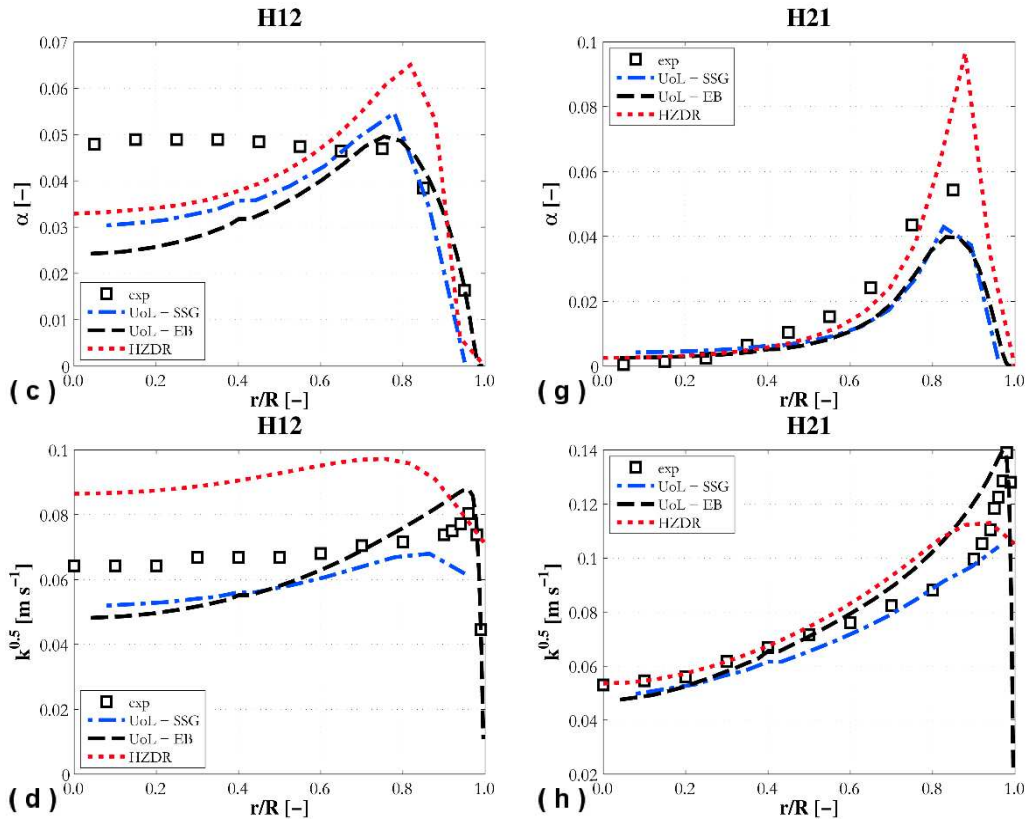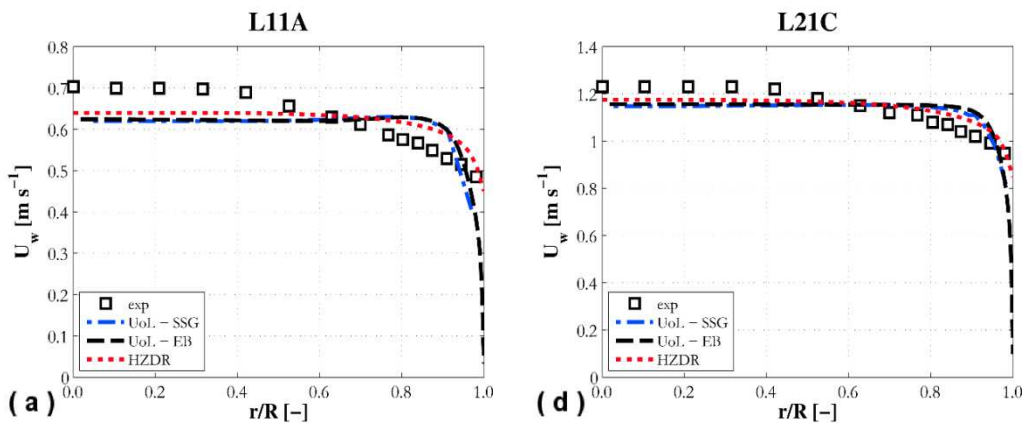| Sub-model	HZDR	UoL SSG	UoL EB
Drag force	Ishii and Zuber [23]	Tomiyama et al. [24]; aspect ratio from Hosokawa and Tomiyama [4]	Tomiyama et al. [24]; aspect ratio from Hosokawa and Tomiyama [4]
Shear lift force	Tomiyama et al. [10]	C_L = 0.10	C_L = 0.10, with cut-off from Shaver and Posowski [26]
Wall force	Hosokawa et al. [12]	Antal et al. [11]	Neglected
Turbulent dispersion force	Burns et al. [28]	Burns et al. [28]	Burns et al. [28]
Virtual mass force	C_{VM} = 0.5	Neglected	Neglected
Base turbulence model	k-ω SST [29]	RSM SSG [30]	RSM SSG [30]
Wall model	Single-phase wall law	Single-phase wall law	Elliptic Blending [31]
Bubble-induced turbulence	Rzehak and Krepper [18]	Rzehak and Krepper [18] with 0.25 coefficient in k source	Rzehak and Krepper [18] with 0.25 coefficient in k source

4. RESULTS AND DISCUSSION

Figure 1. Comparison of CFD predictions from the three models against the radial profiles of liquid velocity (a and e), relative velocity (b and f), void fraction (c and g) and turbulence kinetic energy (d and h) from the experiments of Hosokawa and Tomiyama [4].

Results of the simulations are summarized in Figures 1 to 3. Specifically, Figure 1 shows radial profiles of the average liquid velocity, relative velocity, bubble volume fraction and turbulence kinetic energy for cases H12 and H21. Figure 2 gives the radial liquid velocity, void fraction and turbulence profiles for cases 11A and 21C. Finally, average air velocity and void fraction radial profiles for MT041 and MT061 are shown in Figure 3. Overall, all three models show good accuracy and robustness over the entire dataset, and the better performance of one with respect to another depends on the experiment considered. Velocity and void fraction radial profiles are generally in good agreement with experiments. Larger discrepancies are found in the turbulence predictions, although the accuracy of the models in this regard can still be considered acceptable.
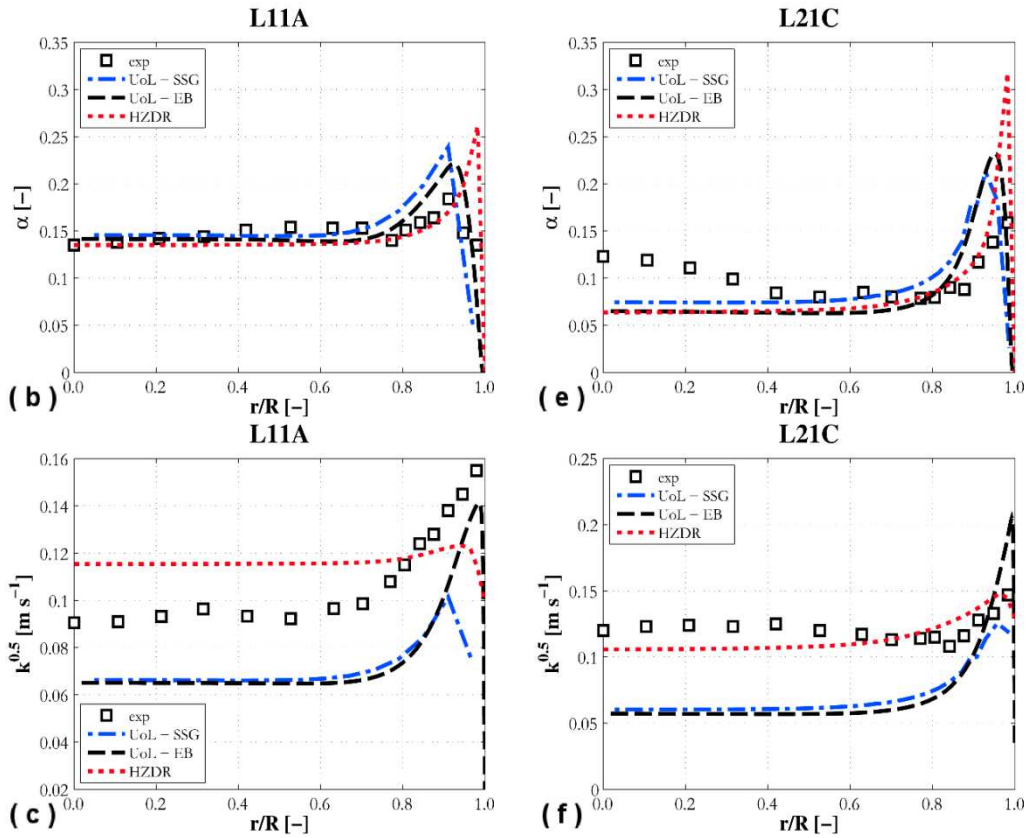
Figure 2. Comparison of CFD predictions from the three models against the radial profiles of liquid velocity (a and d), void fraction (b and e) and turbulence kinetic energy (c and f) from the experiments of Liu [19].

Between the three approaches, the UoL EB model is the newest and by far the least-validated. Its accuracy is found to be generally good, and its generality and applicability promising. Most importantly, the magnitude and location of the void peak is well-predicted over the whole database, even without the addition of a wall force. By resolving the turbulence in the near-wall region, the model predicts the effect of the pressure gradient induced by the radial stress near the wall that pushes bubbles away from the wall [17]. In the following, these results are analysed and discussed further with respect to the different physical quantities considered and the differences in the closures employed by the models.

Liquid and gas radial velocity profiles are generally in good agreement with experiments, although some differences between the models can be identified. The near wall modelling used in the UoL EB model captures very well the near-wall velocity profile, but only for the Hosokawa and Tomiyama [4] experiments (Figure 1(a) and (e)). At higher void fractions (Figure 2(a) and (d)), the model underpredicts the velocity at the last measurement point, with the HZDR model being more accurate. This may be due to some two-phase effects at high void fraction that are still missed by the EB model. However, the velocity in the experiments seems not to approach zero at the wall , and additional testing is required. In the MTLoop experiment (Figure 3(a) and (c)), the air velocity near the wall from the HZDR model is more accurate, suggesting the free-slip boundary condition is to be preferred.

The velocity profiles warrant some discussion on the drag models employed. The UoL models implement the increase in the drag coefficient near the wall from Hosokawa and Tomiyama [4], due to the aspect ratio of the bubbles approaching 1 towards the wall. The relative velocity decrease near the wall agrees very well with the experimental data, even if the bubble aspect ratio is provided by means of an empirical correlation. This effect is not captured by the HZDR

model. Additional testing is, however, necessary, since comparison is limited to the original data used by Hosokawa and Tomiyama [4]. In the centre of the pipe, the UoL models underestimate the relative velocity, while the HZDR drag model is in better agreement (Figure 1(a), (b), (e) and (f)). This underestimation of the relative velocity in the pipe centre by the UoL models remains an open question. Partially, it could be related to the validity of the aspect ratio correlation used which needs further testing.

Prediction of the peak void fraction and the overall void fraction distribution is generally good with all models. At low liquid velocity (H12, L11, MT061; Figures 1(c), 2(b) and 3(d)), the accuracy of the various models is comparable and the void peak well-reproduced. At higher liquid velocity (H21, L21C, MT041; Figures 1(g), 2(e) and 3(b)), the HZDR model overpredicts the magnitude of the void peak. The overestimation of the void peak by the HZDR model is more limited in L21C, which is the experiment with the highest void fraction. In the HZDR model, the Tomiyama correlation [10] gives a constant value of $C_L \approx 0.28$ for $d_B \leq 4.2$ mm, which covers most of the present cases, while both UoL models employ a constant lift coefficient equal to 0.1. However, the differences observed are not only related to these constant values but, most probably, the tendency of the HZDR model to predict excessive bubble migration, as well as the impact of the wall force model and turbulence effects in the near-wall region that may not be captured. In the UoL models, extension from a constant coefficient to a model that accounts for the change in sign in the lift force is required.

As mentioned, inseparable from the action of the shear lift is the role of the wall force. Within the UoL SSG model, the Antal model [11] has a tendency to shift the void fraction peak a little away from the wall, which is particularly noticeable in Figures 2(b), 3(b) and 3(d). This is most surely a consequence of the optimization of the coefficients, since the model was shown in [13] to have a weaker impact than the Hosokawa et al. [12] approach. In contrast, the HZDR model has an opposite tendency to shift the peak towards the wall, particularly in L11A (Figure 2(b)) and L21C (Figure 2(e)). This confirms that, in some cases, a weak wall force can contribute towards an overpredicted void peak. The UoL EB model, without any wall force, shows a more accurate peak position. However, the model will need extension to include some wall force in the limit of a laminar flow, when no turbulence effects will be present.

Finally, we examine the turbulence predictions from the three models, with data available for Hosokawa and Tomiyama [4] (H12 and H21) and Liu [19] (L11A and L21C). None of the models shows any evident accuracy advantage. In the centre of the pipe, the UoL models are more accurate in H12 (Figure 1(d)). In contrast, the HZDR model is more accurate in L21C (Figure 2(f)). All models successfully predict H21 (Figure 1(h)), but none can predict L11A (Figure 2(c)). The UoL models employ the same formulation from [18] used in the HZDR model. The only modification is a constant that limits the production of turbulence kinetic energy. Therefore, the UoL models always predict a lower turbulence kinetic energy with respect to the HZDR approach. Near the wall, both underpredict the peak in the turbulence, as expected by using the wall law. The HZDR model is always the most accurate in this regard. Significant near-wall improvements are obtained with the UoL EB model. The peak in the turbulence kinetic energy is always well captured, except perhaps for L21C. Overall, the dependency on the accuracy of the predicted flow conditions suggests that a more complex modelling of the bubble-induced contribution is required, and HZDR are currently working towards an improved formulation. Considering the impact of the turbulence on the void fraction distribution, a move to Reynolds stress turbulence models is desirable since accurate prediction of the radial stress, specifically near the wall, can only be obtained by capturing the anisotropy of the turbulence. Recently, HZDR has indeed started the development of an RSM that can be coupled to its baseline closure framework [35].
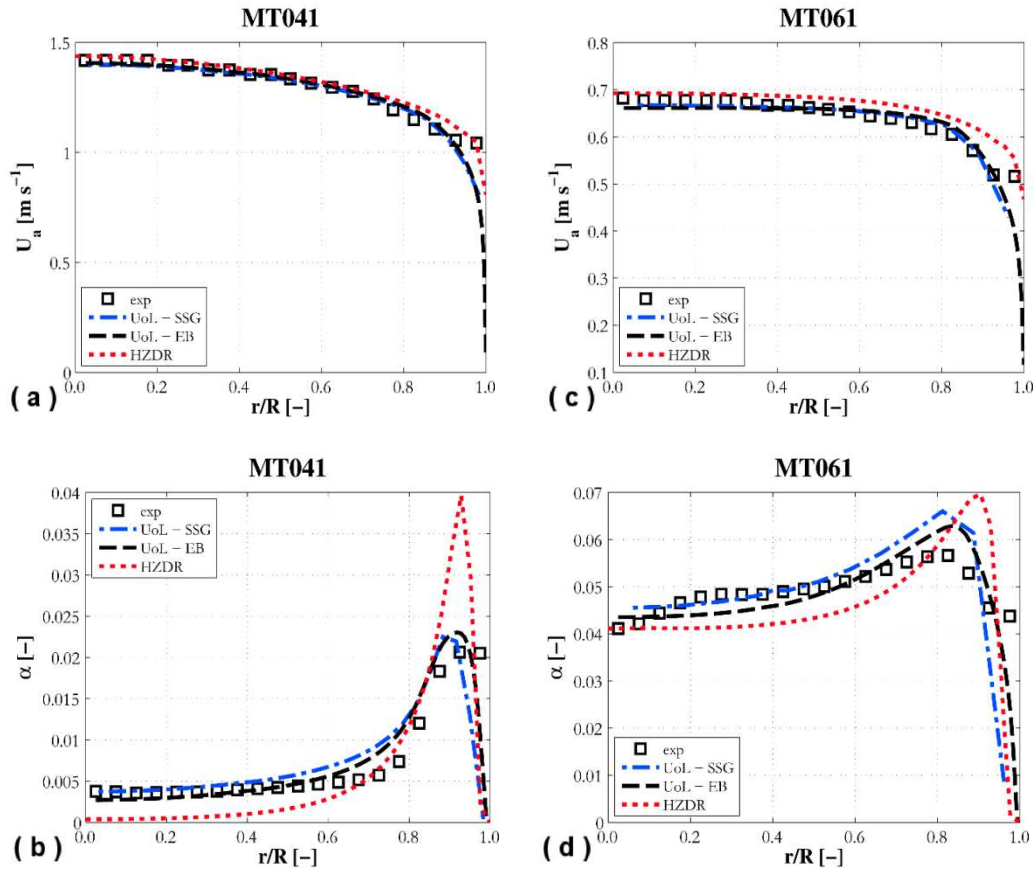
Figure 3. Comparison of CFD predictions from the three models against the radial profiles of gas velocity (a and c) and void fraction (b and d) from the MTLoop experiments [20].

5. CONCLUSIONS

In this work, a blind benchmark of the baseline closure model of HZDR and two, two-fluid Eulerian-Eulerian CFD models from UoL has been carried out. Specifically, different closures for interfacial forces and turbulence models were tested over a database of six bubbly flows characterized by a monodispersed bubble size distribution. Overall, the three models are all capable of good accuracy and robust predictions of bubbly pipe flows. However, additional improvements in different areas were identified. The two models from the UoL return comparable predictions except for the near-wall region. Resolution of this region with the EB-RSM, although in need of further investigation, provides improved accuracy, allowing prediction of the void fraction peak near the wall without the need for any wall force. In view of this, and the significant but not prohibitive computational requirements, the UoL EB is preferable with respect to the UoL SSG model. However, the UoL SSG could still be used with sufficient confidence in cases with particularly high computational requirements.

The drag model employed by HZDR provides the best accuracy. In future, the modification proposed by Hosokawa and Tomiyama in the near-wall region [4] will be further tested. The main features of the lateral void fraction distribution were consistently predicted by all the models. The coupled shear-wall lift modelling in the HZDR approach has a tendency to favour bubble accumulation near the wall at high liquid velocities. The UoL EB model predicted the magnitude and position of the void fraction peak with accuracy and consistency, but extension of the model beyond a constant coefficient is required to extend its applicability to polydispersed bubbly flows. In terms of turbulence modelling, a transition to RSM models is to be encouraged. Additional improvements to models of bubble-induced turbulence, starting from the new HZDR model, will also be pursued by the two research groups.

The benefits of benchmarking exercises of this kind to the accuracy and reliability of our computational models are evident, and additional and larger versions are desirable. Given the number of experiments of different uncertainty available, selection of specific sets of proven measurements that can be used as a reference by the entire research community seems the most promising way forward.

REFERENCES

1. D. Bestion, "Applicability of two-phase CFD to nuclear reactor thermalhydraulics and elaboration of Best Practice Guidelines", Nuclear Engineering and Design, **253**, pp. 311-321 (2012).
2. M. Colombo and M. Fairweather, "RANS simulation of bubble coalescence and break-up in bubbly two-phase flows", Chemical Engineering Science, **146**, pp. 207-225 (2016).
3. J. Feng and I.A. Bolotnov, "Evaluation of bubble-induced turbulence using direct numerical simulation", International Journal of Multiphase Flow, **93**, pp. 92-107 (2017).
4. S. Hosokawa and A. Tomiyama, "Multi-fluid simulation of turbulent bubbly pipe flow", Chemical Engineering Science, **64**, pp. 5308-5318 (2009).
5. Y. Liao, R. Rzehak, D. Lucas and E. Krepper, "Baseline closure model for dispersed bubbly flow: Bubble coalescence and breakup", Chemical Engineering Science, **122**, pp. 336-349 (2015).
6. R. Rzehak, T. Ziegenhein, P. Kriebitzsch, E. Krepper and D. Lucas, "Unified modelling of bubbly flows in pipes, bubble columns, and airlift columns", Chemical Engineering Science, **157**, pp. 147-158 (2017).
7. C. Santarelli and J. Fröhlich, "Direct Numerical Simulations of spherical bubbles in vertical turbulent channel flow. Influence of bubble size and bidispersity", International Journal of Multiphase Flow, **81**, pp. 27-45 (2016).
8. M. Colombo and M. Fairweather, "Multiphase turbulence in bubbly flows: RANS simulations", International Journal of Multiphase Flow, **77**, pp. 222-243 (2015).
9. R. Rzehak, E. Krepper, Y. Liao, T. Ziegenhein, P. Kriebitzsch and D. Lucas, "Baseline model for the simulation of bubbly flows", Chemical Engineering and Technology, **38**, pp. 1972-1978 (2015).
10. A. Tomiyama, H. Tamai, I. Zun and S. Hosokawa, "Transverse migration of single bubbles in simple shear flows", Chemical Engineering Science, **57**, pp. 1849-1858 (2002).
11. S.P. Antal, R.T. Lahey and J.E. Flaherty, "Analysis of phase distribution in fully developed laminar bubbly two-phase flow", International Journal of Multiphase Flow, **17**, pp. 635-652 (1991).
12. S. Hosokawa, A. Tomiyama, S. Misaki and T. Hamada, "Lateral migration of single bubbles due to the presence of wall", ASME Joint U.S.-European Fluids Engineering Division Conference (FEDSM), Montreal, Canada (2002).
13. R. Rzehak, E. Krepper and C. Lifante, "Comparative study of of wall-force models for the simulation of bubbly flows", Nuclear Engineering and Design, **253**, pp. 41-49 (2012).
14. T. Hibiki and M. Ishii, "Lift force in bubbly flow systems", Chemical Engineering Science, **62**, pp. 6457-6474 (2007).
15. Y. Liao, T. Ma, L. Liu, T. Ziegenhein, E. Krepper and D. Lucas, "Eulerian modelling of turbulent bubbly flow based on a baseline closure concept", Nuclear Engineering and Design, **337**, pp. 450-459 (2018).

16. D. Lucas, R. Rzehak, E. Krepper, T. Ziegenhein, Y. Liao, P. Kriebitzsch and P. Apanasevich, "A strategy for the qualification of multi-fluid approaches for nuclear reactor safety", Nuclear Engineering and Design, **299**, pp. 2-11 (2016).
17. M. Colombo and M. Fairweather, "Influence of multiphase turbulence modelling on interfacial momentum transfer in two-fluid Eulerian-Eulerian CFD models of bubbly flows", Chemical Engineering Science, **195**, pp. 968-984 (2019).
18. R. Rzehak and E. Krepper, "CFD modeling of bubble-induced turbulence", International Journal of Multiphase Flow, **55**, pp. 138-155 (2013).
19. T.J. Liu, "The role of bubble size on liquid phase turbulent structure in two-phase bubbly flow", 3rd International Conference on Multiphase Flow (ICMF1998), Lyon, France (1998).
20. D. Lucas, E. Krepper and H.M. Prasser, "Development of co-current air-water flow in a vertical pipe", International Journal of Multiphase Flow, **31**, pp. 1304-1328 (2005).
21. M. Ishii and T. Hibiki, Thermo-fluid dynamics of two-phase flow, Springer, New York, USA (2006).
22. G.H. Yeoh and J.Y. Tu, Computational techniques for multiphase flows - Basics and applications, Butterworth-Heinemann, Elsevier, Oxford, United Kingdom (2010).
23. M. Ishii and N. Zuber, "Drag coefficient and relative velocity in bubbly, droplet or particulate flows", AIChE Journal, **25**, pp. 843-855 (1979).
24. A. Tomiyama, G.P. Celata, S. Hosokawa and S. Yoshida, "Terminal velocity of single bubbles in surface tension dominant regime", International Journal of Multiphase Flow, **28**, pp. 1497-1519 (2002).
25. R.M. Welleck, A.K. Agrawal and A.H.P. Skelland, "Shape of liquid drops moving in liquid media", AIChE Journal, **12**, pp. 854-862 (1966).
26. D.R. Shaver and M.Z. Podowski, "Modeling of interfacial forces for bubbly flows in subcooled boiling conditions", Transaction of the American Nuclear Society, **113**, pp. 1368-1371 (2015).
27. N. Lubchenko, B. Magolan, R. Sugrue and E. Baglietto, "A more fundamental wall lubrication force from turbulent dispersion regularization for multiphase CFD applications", International Journal of Multiphase Flow, **98**, pp. 36-44 (2018).
28. A.D. Burns, T. Frank, I. Hamill and J.M. Shi, "The Favre averaged drag model for turbulent dispersion in Eulerian multi-phase flows", 5th International Conference on Multiphase Flows, Yokohama, Japan, May 30 - June 4 (2004).
29. F.R. Menter, "Review of the shear-stress transport turbulence model experience from an industrial perspective", International Journal of Computational Fluid Dynamics, **23**, pp. 305-316 (2009).
30. C.G. Speziale, S. Sarkar and T.B. Gatski, "Modelling the pressure-strain correlation of turbulence: An invariant dynamical system approach", Journal of Fluid Mechanics, **227**, pp. 245-272 (1991).
31. R. Manceau, "Recent progress in the development of the Elliptic Blending Reynolds-stress model", International Journal of Heat and Fluid Flow, **51**, pp. 195-220 (2015).
32. M. Lopez de Bertodano, S.J. Lee, R.T. Lahey Jr. and D.A. Drew, "The prediction of two-phase turbulence and phase distribution phenomena using a Reynolds stress model", Journal of Fluids Engineering, **112**, pp. 107-113 (1990).
33. ANSYS, ANSYS CFX-solver theory guide release 14.5, ANSYS Inc. (2012).
34. CD-adapco, STAR-CCM+® Version 10.04 User Guide (2016).
35. J. Parekh and R. Rzehak, "Euler-Euler multiphase CFD-simulation with full Reynolds stress model and anisotropic bubble-induced turbulence", International Journal of Multiphase Flow, **99**, pp. 231-245 (2018).